Available online at www.sciencedirect.com

ScienceDirect

Procedia Structural Integrity 28 (2020) 784–789

Structural Integrity Procedia

www.elsevier.com/locate/procedia

1st Virtual European Conference on Fracture

Numerical modelling of cracking in gravity dam under static and seismic loadings with multiple pre-embedded discontinuity FEM

Timo Saksala*, Jari Mäkinen

Civil Engineering, Tampere University, Tampere, FI-33014, Finland

Abstract

This paper presents a numerical study on the earthquake analysis of a concrete gravity dam. The numerical approach is based on the multiple pre-embedded discontinuity finite element method. The equations of motion with the ground motion excitation, static self-weight, hydrostatic reservoir load and the hydrodynamic reservoir loads as the boundary conditions are solved with explicit time stepping. Mass proportional damping is used instead of the usual stiffness proportional damping since the latter drastically decreases the critical time step of explicit time integration. The Koyna dam with the genuine accelerograms recorded during the 1967 earthquake is analyzed as the numerical example. The simulation results agree with the previously reported results by other studies, i.e. similar crack propagation in the monolith is predicted here.

Keywords: Concrete dams; Concrete fracture; Earthquake; Embedded discontinuity finite elements

1. Introduction

Failure analysis of gravity dams is a task of utmost importance in Civil and Geotechnical Engineering. One of the most challenging aspects therein is to predict the cracking behavior of a concrete dam under earthquake induced ground motion. This has been the topic of many numerical studies (Lee and Fenves 1998; Alembagheri 2016; Udni and Bouafia 2015; Chopra and Chakrabarti 1972 & 1973, for example) since the Koyna earthquake (1967), which

* Corresponding author. Tel.: +358451302950; fax: +0-000-000-0000 .
E-mail address: timo.saksala@tuni.fi

10.1016/j.prostr.2020.10.091

lead to extensive damage of the nearby Koyna gravity dam Chopra and Chakrabarti (1973). Most of these studies are based on damage-plasticity models, which model the cracking in a smeared sense, as a localized deformation.

In the present study, we apply the embedded discontinuity finite elements approach in analyzing a concrete dam under hydrostatic loading due to reservoir with an overflow situation and due earthquake ground motion. The embedded discontinuity approach, which enriches the standard finite element with a displacement discontinuity, is superior to continuum damage and plasticity models in crack description while retaining the computational efficiency of continuum models. The purpose of this 2D numerical study is to demonstrate the performance of the specific model for concrete by Saksala (2018) in the earthquake analysis of a gravity dam, namely the Koyna dam during the 1967 earthquake.

2. Theory of the concrete fracture model

Concrete fracture is described by the embedded discontinuity approach. In this method, the crack is represented by a displacement discontinuity embedded inside a finite element. In the present multiple discontinuity version (Saksala 2018), three intersecting discontinuities are pre-embedded (before analysis) inside each finite element parallel to its edges. For the constant strain triangle (CST) element, the displacement, $\mathbf{u}$, and strain, $\boldsymbol{\varepsilon}$, fields can be written as

$$\begin{aligned}
&\mathbf{u} = N_i \mathbf{u}_i^e + \textstyle\sum_{k=1}^{3} (H_{\Gamma_d}^k - \varphi_k)\boldsymbol{\alpha}_d^k \\
&\boldsymbol{\varepsilon} = (\nabla N_i \otimes \mathbf{u}_i^e)^{sym} - \textstyle\sum_{k=1}^{3} \left((\nabla \varphi_k \otimes \boldsymbol{\alpha}_d^k)^{sym} + \delta_{\Gamma_d}^k (\mathbf{n}_k \otimes \boldsymbol{\alpha}_d^k)^{sym} \right) \quad \text{with} \\
&\mathbf{n}_k = \nabla N_k / \left\| \nabla N_k \right\|, \quad \varphi_k = N_k
\end{aligned} \tag{1}$$

where $\boldsymbol{\alpha}_d^k$ is the displacement jump vector, N_i and $\mathbf{u}_i^e$ are the standard interpolation function and displacement vector at node i (summation applies on repeated i), and $H_{\Gamma_d}^k$ and $\delta_{\Gamma_d}^k$ is the Heaviside and Dirac's delta function at discontinuity k with normal $\mathbf{n}_k$. Moreover, φ_k is a function that restricts the effect of the displacement jump $\boldsymbol{\alpha}_d^k$ within the corresponding finite element facilitating the treatment of the essential boundary conditions. It should be mentioned that the gradient of the displacement jump is assumed zero here, i.e. constant mode I and II discontinuity is adopted. Equations (1) specify also how functions φ_k and normals $\mathbf{n}_k$ are calculated based on interpolation functions.

Next, a model controlling the crack opening and the corresponding traction vector for each crack needs to be specified. Here, the plasticity inspired model by Saksala (2018) is employed for solving the displacement jump (crack opening) and traction vector updates. This model is specified by following components

$$\begin{aligned}
&\phi_i(\mathbf{t}_{\Gamma_d}^i, \kappa_i, \dot{\kappa}_i) = \mathbf{n}_i \cdot \mathbf{t}_{\Gamma_d}^i + \beta \,|\, \mathbf{m}_i \cdot \mathbf{t}_{\Gamma_d}^i \,| - (\sigma_t + q_i(\kappa_i, \dot{\kappa}_i)) \\
&q_i = h_i \kappa_i + s\dot{\kappa}_i, \quad h_i = -g\sigma_t \exp(-g\kappa_i), \quad g = G_{Ic} / \sigma_t \\
&\dot{\mathbf{t}}_{\Gamma_d}^i = -\mathbf{E} : \textstyle\sum_{k=1}^{3} (\nabla N_k \otimes \dot{\boldsymbol{\alpha}}_d^k)^{sym} \cdot \mathbf{n}_i \quad \dot{\boldsymbol{\alpha}}_d^i = \dot{\lambda}_i \dfrac{\partial \phi_i}{\partial \mathbf{t}_{\Gamma_d}^i}, \quad \dot{\kappa}_i = -\dot{\lambda}_i \dfrac{\partial \phi_i}{\partial q_i} \\
&\dot{\lambda}_i \geq 0, \quad \phi_i \leq 0, \quad \dot{\lambda}_i \phi_i = 0, \quad i, j = 1,2,3
\end{aligned} \tag{2}$$

where $\mathbf{m}_i$ is the unit tangent vector of discontinuity i, $\kappa_i, \dot{\kappa}_i$ are the are the internal variable and its rate related to the softening law for a discontinuity, and σ_t and s are the tensile strength and the viscosity of the material. Moreover, h_i is the softening modulus of the exponential softening rule, and parameter g controls the initial slope of the softening curve and is calibrated by the mode I fracture energy G_{Ic}. Finally, β is a parameter that controls the effect of shear (mode-II) component of the traction vector. The evolution of the traction vectors is based on the Cauchy expression of traction as an inner product between the stress tensor and the crack normal. This relation, defining the stress-strain relationship as well, reads

$$\mathbf{t}_{\Gamma_d}^i = \boldsymbol{\sigma} : \mathbf{n}_i = \left(\mathbf{E} : (\dot{\overline{\boldsymbol{\varepsilon}}} - \textstyle\sum_{k=1}^{3} (\nabla N_k \otimes \dot{\boldsymbol{\alpha}}_d^k)^{sym}) \right) \cdot \mathbf{n}_i \tag{3}$$

where $\bar{\boldsymbol{\varepsilon}} = (\nabla N_i \otimes \mathbf{u}_i^e)^{sym}$, i.e. the regular finite element strain tensor, which is kept constant during local iteration.

The material behavior thus described is locally isotropic and linearly elastic until the tensile strength is reached after which the model described by Equations (2) governs the post-peak softening process. The last inequalities in Equations (2) are the classical Kuhn-Tucker conditions that impose the consistency. This formulation enables to solve Equations (2) with standard methods of computational plasticity while the rate-dependency of concrete is accommodated by viscosity.

3. Solution of equations of motion with ground motion BC

The global equations of motions with the ground motion boundary condition are solved with explicit time marching in a standard manner. Hence, the system of equations and the forward Euler based scheme to proceed further in time are written as

$$\begin{aligned} &\mathbf{M}\ddot{\mathbf{u}}_t + \mathbf{C}\dot{\mathbf{u}}_t + \mathbf{f}_{\text{int},t}(\mathbf{u}_t, \dot{\mathbf{u}}_t) = -\mathbf{M}\mathbf{L}\ddot{\mathbf{u}}_t^g + \mathbf{f}_{\text{ext},t} \rightarrow \ddot{\mathbf{u}}_t \\ &\dot{\mathbf{u}}_{t+1} = \dot{\mathbf{u}}_t + \Delta t\ddot{\mathbf{u}}_t, \quad \mathbf{u}_{t+1} = \mathbf{u}_t + \Delta t\dot{\mathbf{u}}_{t+1} \end{aligned} \tag{4}$$

where $\mathbf{M}$, $\mathbf{C}$ and $\mathbf{K}$ are, respectively, the lumped mass matrix, the damping matrix and linear elastic stiffness matrix, $\mathbf{f}_{\text{int}}$ is the internal force vector depending on the displacement and velocity, $\mathbf{L}$ is the influence matrix for the ground motion acceleration $\ddot{\mathbf{u}}^g$, and $\mathbf{f}_{\text{ext}}$ is the external force vector containing contributions from the self-weight of the dam and the hydrostatic forces due to reservoir. Rayleigh mass proportional damping is used in (4), i.e. $\mathbf{C} = \alpha\mathbf{M}$ with α being the proportionality factor. The reason for mass, instead of stiffness, proportional damping is that the stiffness proportional damping drastically decreases the critical time step of explicit time integration. Finally, $\mathbf{u}_t, \dot{\mathbf{u}}_t, \ddot{\mathbf{u}}_t$ are the displacement, velocity and acceleration vectors at time t. The influence matrix is calculated with the linear elastic stiffness matrix by $\mathbf{L} = -\mathbf{K}_{\text{act}}^{-1}\mathbf{K}_g$, where $\mathbf{K}_{\text{act}}$ and $\mathbf{K}_g$ are the parts of the stiffness matrix corresponding to the superstructure and the support nodes, respectively (Villaverde 2009). The hydrodynamic forces are accounted for with the added mass technique by Westergaard (1933).

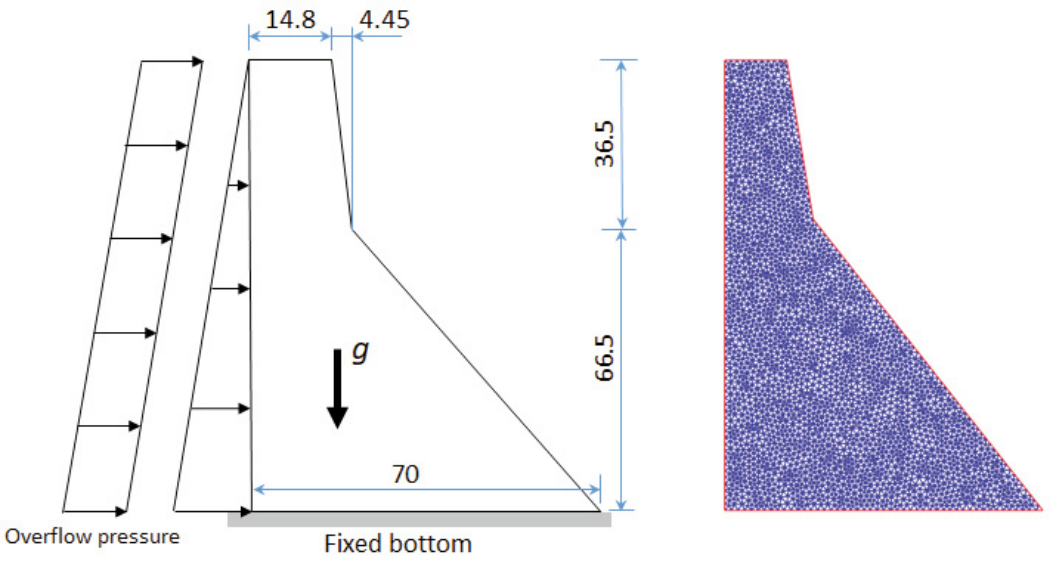

Fig. 1. (a) Dimensions and boundary conditions of the Koyna dam model under quasi-static loading; (b) the finite element mesh with 5364 CST triangles.

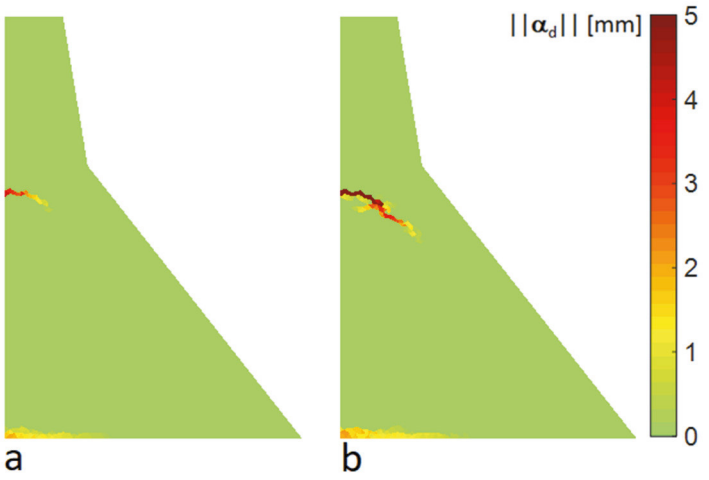

Fig. 2. (a) crack propagation when p_{of} = 195 kPa; (b) crack propagation when p_{of} = 260 kPa.

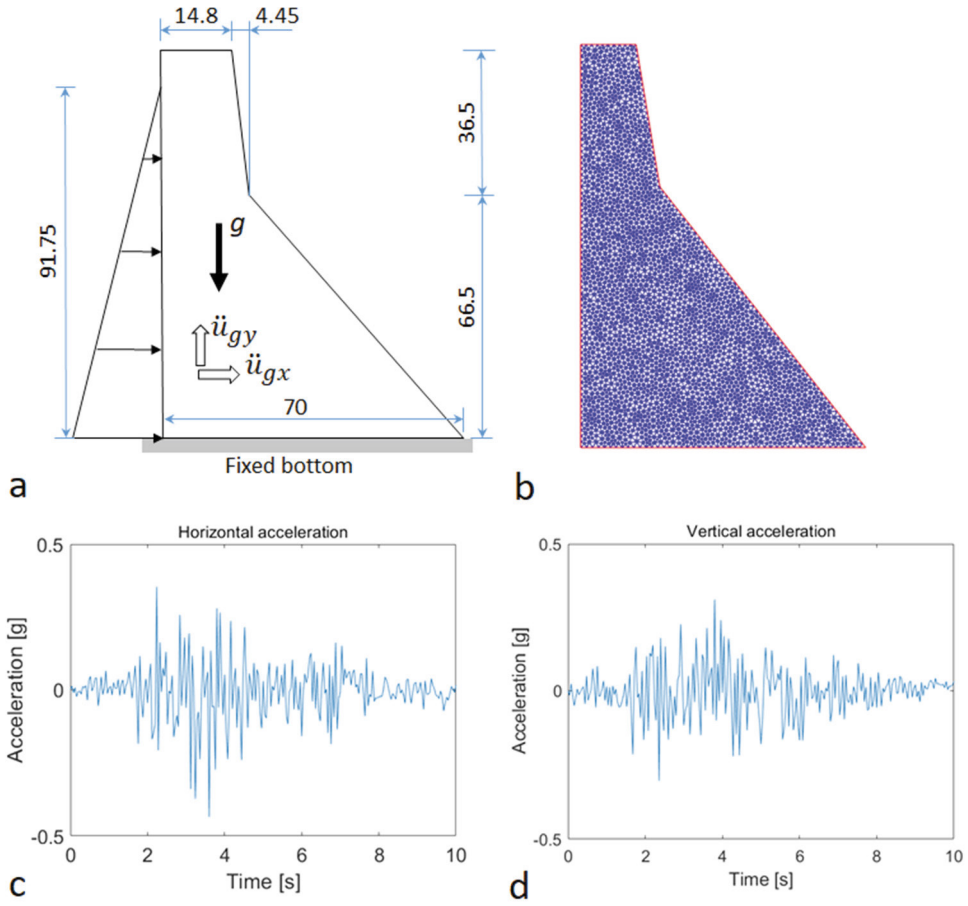

Fig. 3. (a) Dimensions and boundary conditions of the Koyna dam model; (b) the finite element mesh with 5364 CST triangles; (c) the horizontal accelerogram; (d) vertical accelerograms for simulations.

4. Numerical examples

4.1. Koyna dam under quasi-static loading

The first example concerns the Koyna dam under self-weight, full reservoir load and an overflow situation shown in Fig. 1. The material properties for concrete (taken from Jirasek and Zimmerman (2001)) and the model parameters are as follows: $E = 25$ GPa, $\nu = 0.2$, $\rho = 2643$ kg/m^3, $\sigma_t = 1$ MPa, $G_{Ic} = 200$ N/m, $s = 0.1$ MPas/m, and $\beta = 0.75$. The overflow pressure is increased linearly during simulation until cracks develop. The simulation results at two stages of crack propagation due to increasing in overflow-induced pressure are shown in Fig. 2.

According to the crack propagation results presented in terms of the crack opening magnitude, the first crack appears at the upstream corner of the base where the bending (tensile) stress is at its maximum. Then, the second crack appears higher in the upstream face and propagates into the monolith with a curved trajectory. This secondary crack is roughly similar to that reported by Jirasek and Zimmermann (2001) in their numerical study.

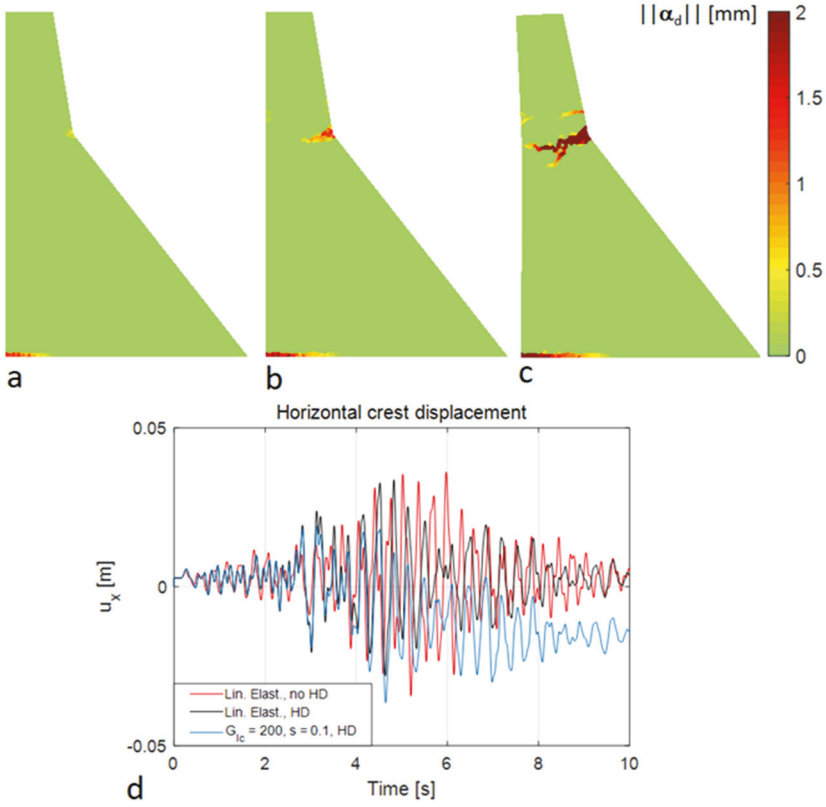

Fig. 4. Simulation results: (a) crack opening magnitude at t = 2.8 s; (b) at t = 3.93 s; (c) at the end of analysis in deformed mesh (magnification = 100); (d) the dam crest horizontal movement as a function of time.

4.2. Koyna dam under static and dynamic loading

The second example concerns the Koyna dam under the ground accelerations recorded during the 1967 earthquake as well as the self-weight and the hydrostatic reservoir load. The dam dimensions, boundary conditions and finite element mesh are illustrated in Fig. 3. The reservoir height is 91.75 m.

The material properties (taken from Abaqus Examples Guide 2014) for concrete and the model parameters are as follows: $E = 31$ GPa, $\nu = 0.15$, $\rho = 2643$ kg/m^3, $\sigma_t = 2.4$ MPa, $G_{Ic} = 200$ N/m, $s = 0.1$ MPas/m, and $\beta = 0.75$. As for the Rayleigh damping proportionality factor, Abaqus Example Guide (2014) is followed assuming 3% fraction of

critical damping for the first mode of vibration of the dam. This, with the $\omega_1 = 18.61$ rad/s for the Koyna dam (see Abaqus 6.14 Example Guide), gives $\alpha = 2 \cdot 0.03 \omega_1 = 1.12$.

According to the simulation results in Fig. 4a, the dam fails first at its upstream corner of the base where the bending (tensile) stress due to the hydrostatic reservoir load is at its maximum. Then, when the heavier oscillations in the ground motion due to the earthquake start, a crack initiates at the geometry induced stress concentration on the downstream face, as can be observed in Fig. 4a and b. This crack propagates further to upstream direction and, after reaching the half way through the monolith, branching occurs (Fig. 4c). However, the main branch of the crack does not reach the upstream face of the dam. Moreover, some secondary cracking is attested in Fig. 4c. Most of these cracking events took place during the major oscillations in the ground motion, i.e. between 2 and 5 seconds of time, after which the cracks remained stable. Generally, the cracking behavior predicted here agrees with the results reported by Lee and Fenves (1998) and Abaqus Example Problems Guide (2014).

As to the horizontal crest movement plotted in Fig. 4d, the irreversible nature of the present crack model is attested in the results as the final displacement of the crest oscillates around 1.5 mm of final upstream displacement.

4. Conclusion

A computational framework for numerical analysis of dam fracturing was presented in this paper. The crack modelling approach was based on the multiple embedded discontinuity finite elements. As the discontinuities are pre-embedded parallel to the edges of each triangle element in the mesh, this approach is somewhat similar to the cohesive interface element approach. However, in contrast to the cohesive zone elements, here the extra variables, i.e. the crack opening vectors, are totally local in nature so that they can either be eliminated by static condensation or treated similarly as the plastic strain tensor in plasticity models. Thereby, the present approach is computationally cheaper than cohesive zone interphase element methods.

The present model was tested in simulations of the Koyna dam under quasi-static loading due to full reservoir and an overflow and under the earthquake that lead to extensive damage of the monolith in 1967. The simulation results demonstrated that the present approach can predict the salient features of a gravity dam under both the quasi-static loading and seismic excitation. Specifically, the cracking behavior predicted here is generally similar to the one predicted with damage-plasticity models by previous studies. Therefore, the present approach could be a tool in earthquake engineering, especially after a future extension to 3D.

Acknowledgements

This research was funded by Academy of Finland under grant number 298345.

References

Abaqus 6.14 Example Problems Guide, Simulia, Dassault Systemes, 2014.

Alembagheri, M., 2016. Earthquake damage estimation of concrete gravity dams using linear analysis and empirical failure criteria. Soil Dynamics and Earthquake Engineering 90:327–339.

Chopra A.K., Chakrabarti, P., 1972. The Earthquake Experience at Koyna Dam and Stresses in Concrete Gravity Dams. International Journal of Earthquake Engineering and Structural Dynamics 1:151-164.

Chopra A.K., Chakrabarti, P., 1973. The Koyna Earthquake and the Damage to Koyna Dam. Bulletin of the Seismological Society of America 63:381-397.

Jirasek, M., Zimmermann, T., 2001. Embedded crack model. Part II: Combination with smeared cracks. International Journal for Numerical Methods in Engineering 50:1291–1305.

Lee, J., Fenves, G.L., 1998. A plastic-damage concrete model for earthquake analysis of dams. Earthquake Engineering and Structural Dynamics, 27:937–56.

Saksala, T., 2018. Numerical modelling of concrete fracture processes under dynamic loading: meso-mechanical approach based on embedded discontinuity finite elements. Engineering Fracture Mechanics 201: 282-297.

Udni, N., Bouafia, Y., 2015. Response of concrete gravity dam by damage model under seismic excitation. Engineering Failure Analysis 58:417–428.

Villaverde, R., 2009. Fundamental Concepts of Earthquake Engineering. CRC Press, Taylor & Francis, Boca Raton, USA.

Westergaard, H. M., 1933. Water pressure on dams during earthquakes. Transactions of the American Society of Civil Engineers 98, 418–472.